

Research Article

Open Access



# Effects of solutes on thermodynamic properties of (TMZrU)C (TM = Ta, Y) medium-entropy carbides: a first-principles study

Ya Liu<sup>1,2</sup>, Yonghong Lu<sup>3</sup>, William Yi Wang<sup>1,2,\*</sup> , Jia Li<sup>1,2</sup>, Ying Zhang<sup>1,2</sup>, Junlei Yin<sup>1,2</sup>, Xiaoqiang Pan<sup>3</sup>, Xingyu Gao<sup>4,\*</sup>, Yong Chen<sup>3</sup>, Haifeng Song<sup>4</sup>, Jinshan Li<sup>1,2,\*</sup>

<sup>1</sup>State Key Laboratory of Solidification Processing, Northwestern Polytechnical University, Xi'an 710072, Shaanxi, China.

<sup>2</sup>Innovation Center, NPU Chongqing, Chongqing 401135, China.

<sup>3</sup>Nuclear Power Institute of China, Chengdu 610213, Sichuan, China.

<sup>4</sup>Laboratory of Computational Physics, Institute of Applied Physics and Computational Mathematics, Beijing 100094, China.

**\*Correspondence to:** Prof. William Yi Wang, Prof. Jinshan Li, State Key Laboratory of Solidification Processing, Northwestern Polytechnical University, 127 West Youyi Road, Beilin District, Xi'an 710072, Shaanxi, China. E-mail: wywang@nwpu.edu.cn; ljsh@nwpu.edu.cn; Prof. Xingyu Gao, Laboratory of Computational Physics, Institute of Applied Physics and Computational Mathematics, Fenghao East Road No. 2, Haidian District, Beijing 100094, China. E-mail: gao\_xingyu@iapcm.ac.cn

**How to cite this article:** Liu Y, Lu Y, Wang WY, Li J, Zhang Y, Yin J, Pan X, Gao X, Chen Y, Song H, Li J. Effects of solutes on thermodynamic properties of (TMZrU)C (TM = Ta, Y) medium-entropy carbides: a first-principles study. *J Mater Inf* 2023;3:17. <https://dx.doi.org/10.20517/jmi.2023.19>

**Received:** 15 May 2023 **First Decision:** 14 Jul 2023 **Revised:** 7 Aug 2023 **Accepted:** 15 Aug 2023 **Published:** 22 Aug 2023

**Academic Editor:** Xingjun Liu **Copy Editor:** Dong-Li Li **Production Editor:** Dong-Li Li

## Abstract

High entropy carbide ceramics have garnered significant interest as a novel class of ultra-high temperature and superhard metallic materials. In the present work, a comparative investigation was conducted for the first time on the stability, mechanical, and thermodynamic properties of two medium entropy carbides (MECs), (TaZrU)C and (YZrU)C, using high-throughput first-principles calculations. Additionally, data from groups IV and V transition metal monocarbides were employed for comparison. The temperature-dependent thermodynamic properties, including bulk modulus (B), constant volume/constant pressure heat capacity (Cv/Cp), Gibbs free energy, volume, entropy, and thermal conductivity, were evaluated using the Debye-Gruneisen model. The results demonstrate that (TaZrU)C and (YZrU)C exhibit similar trends in their thermodynamic properties, with (YZrU)C displaying slightly superior performance as the temperature rises. This work provides valuable insights into the design of innovative high entropy fuels, holding significant implications for the advancement of MEC ceramic fuels in advanced nuclear power systems and nuclear thermal propulsion systems.

**Keywords:** Medium entropy carbide ceramics, first-principles calculations, thermodynamic properties, transition metal monocarbides, nuclear thermal propulsion (NTP) systems



© The Author(s) 2023. **Open Access** This article is licensed under a Creative Commons Attribution 4.0 International License (<https://creativecommons.org/licenses/by/4.0/>), which permits unrestricted use, sharing, adaptation, distribution and reproduction in any medium or format, for any purpose, even commercially, as long as you give appropriate credit to the original author(s) and the source, provide a link to the Creative Commons license, and indicate if changes were made.



## INTRODUCTION

Being one kind of ultra-high temperature ceramics<sup>[1-10]</sup>, transition metal carbide ceramics of the IVB, VB, and VIB groups have found wide applications in various fields, such as hard cutting tools, high-temperature abrasives, aerospace industry, submarine equipment, and nuclear energy<sup>[1,2,10-13]</sup>. They also present several attractive properties, including excellent thermal and electrical conductivity, chemical corrosion resistance, high melting point and hardness, abrasion resistance, oxidation and radiation resistance, and high temperature stability<sup>[14-16]</sup>. In recent years, a new approach to alloy design has emerged with the development of polymetallic solid solution compounds. These alloys, known as high entropy materials (HEMs)<sup>[17-21]</sup>, are formed by combining five or more principal elements, each with a concentration between 35 and 5 at.% and exhibiting a mixing entropy  $S > 1.5R$ . Owing to the contributions of high entropy, HEMs exhibit unique characteristics different from those of metal simple substances, which can be summarized as four major effects, including high entropy effects, sluggish diffusion effects, severe lattice distortion effects, and cocktail effects.

High entropy carbide ceramics (HECs) are single-phase solid solutions composed of four or more transition metal (TM) atoms. Theoretical studies have helped scientists to prepare and study HECs more efficiently and economically through different simulation methods<sup>[22,23]</sup>. For instance, high-throughput computing and machine learning (ML) have been used to study HEMs<sup>[22,24-29]</sup>. Castle *et al.* experimentally fabricated the high entropy carbides (HECs) and inherited the four effects of HEMs<sup>[30,31]</sup>. Medium entropy carbides (MECs) were then derived from the concept of HECs, with a mixing entropy between  $1R$  and  $1.5R$ . MECs, such as HECs, have excellent mechanical and functional properties. The study of the properties of MECs in multicomponent solid solutions has been widely reported<sup>[32-36]</sup>. Compared to traditional binary carbides, HECs and MECs exhibit superior physical and chemical performances, such as high thermal stability, good corrosion resistance, high fracture toughness, high Young's modulus, and high hardness<sup>[24,30,37-42]</sup>.

In the field of nuclear energy, the Nuclear Thermal Propulsion (NTP) engine systems are attractive options for planetary exploration applications due to their high performance, such as Mars exploration<sup>[43-46]</sup>. In order to achieve better performance of NTP systems, the NTP reactors will be utilized at temperatures above 2,500 K and maintaining pressures exceeding 3 MPa. Historically, uranium fuel (UC) has been the primary focus for NTP reactors. The design and study of UC as the initial fuel element have received significant attention<sup>[47-50]</sup>. However, relying solely on UC and UC<sub>2</sub> would impose severe limitations on the core operating temperature, resulting in a reduction in NTP specific impulse<sup>[51]</sup>.

In recent decades, there has been a progression in the development of carbide fuels, transitioning from single-component compositions<sup>[52-57]</sup> to multicomponent compositions, such as (ZrU)C and (ZrNbU)C<sup>[35]</sup>. Notably, Pelaccio *et al.* have designed solid-solution (ZrU)C ceramic fuels, which currently serve as the primary source of nuclear fuel for NTP reactors, offering improved reliability<sup>[58]</sup>. Composite ceramic fuels, including UC or (ZrU)C, exhibit advantageous properties such as high melting point temperatures and high thermal conductivity. Unfortunately, the compatibility of composite ceramics, such as UC or (ZrU)C, with fuse-resistant alloys is limited at higher temperatures. Further exploration of incorporating a third metal atom into the (ZrU)C system holds the potential to unveil the future prospects of carbide fuels, specifically MEC ceramic fuels, for advanced nuclear power systems. Multicomponent (ZrNbU)C fuels are regarded as the preferred choice for realizing high thrust nuclear-powered spacecraft in the future, and in the study, a powder metallurgical process combining carbothermal reduction and liquid phase sintering is used to prepare poly (ZrNbU)C fuels. The mechanisms and laws of the process parameters on the reaction kinetics,

phase structure, thermal conductivity, and microstructure of multi-element (ZrNbU)C fuel are investigated<sup>[59]</sup>. Additionally,  $(U_xZr_{1-x})C_y$  systems exhibit promise as design concepts/strategies for advanced nuclear power systems due to their unique nuclear properties and thermal stability<sup>[60]</sup>.

In the present work, tantalum (Ta) or yttrium (Y) is added as the third metal atom to the (ZrU)C system to explore their effects on the properties of MECs. Proper doping of trace elements has been shown to promote the densification and grain growth of ceramic materials and extend their service life<sup>[61]</sup>. It has been reported that the utilized temperature of (TaZrU)C fuel could be improved by the addition of Ta and Zr into the classical UC one<sup>[62]</sup>, which is selected as the investigated candidacy fuel in the present work. This work investigates the physical property changes and thermodynamic properties of (TMZrU)C (TM = Ta, Y) MECs in detail using high-throughput first-principles calculations, providing valuable data and technical support for the design of new high entropy fuel from both an electronic and atomic perspective. Specifically, we focus on examining the equilibrium volume ( $V_0$ ), Gibbs free energy, constant volume heat capacity ( $C_v$ ), constant pressure heat capacity ( $C_p$ ), bulk modulus ( $B_0$ ), and thermal conductivity of the (TMZrU)C structures. This research holds promise for the advancement of carbide materials, specifically MEC ceramic fuels, with implications for NTP systems.

## MATERIALS AND METHODS

### Multicomponent supercell construction via similar atomic environment

Consideration of the possible quasirandom structure with lattice distortion is important in the modeling of disordered structures. In the present work, the similar atomic environment (SAE) toolkit combined in the Professional Materials at Extreme (ProME) platform is utilized to construct the supercells of the multicomponent system<sup>[63,64]</sup>, which has the capability to systematically screen the optimal structure of the fuel doping system. It is noted that the SAE approach is a novel structural modeling method that employs a similarity function to quantitatively describe the deviation between the current configuration and the desired disordered solid solution structure. This approach enables the construction of quasirandom structures to be transformed into a minimization problem of configuration space. The superlattices of (TaZrU)C and (YZrU)C with 64 atoms were constructed using the SAE method, as shown in [Figure 1](#), based on the cell structures of ZrC (the space group number No. 225 and the lattice parameter  $a = b = c = 4.48 \text{ \AA}$ ) and YC (the space group number No. 225 and the lattice parameter  $a = b = c = 5.09 \text{ \AA}$ ). The supercells were generated by enlarging the unit cell of  $2 \times 2 \times 2$ , which were also selected as representative models to simulate the solid solution alloys under various occupancy conditions. In order to improve the efficiency of structural optimization/selection, two parallel independent calculations were performed. In each optimization loop, the number of random structures conforming to the elemental ratios was first generated to be 1,000, and then the one with the smallest objective function was selected as the seed structure for subsequent optimization. Subsequently, starting with the seed structure, the Metropolis Monte Carlo (MMC) algorithm was used to minimize the objective function and exchange atomic positions to evolve the structure<sup>[63]</sup>. Finally, by repeating the above cycle 12 times, the objective function will reach a local minimum, and the criterion to complete the optimization process is expressed as<sup>[63]</sup>:

$$g(A_m, \sigma) = \sqrt{\frac{1}{N(A_m^\sigma)} \sum_{A_m^\sigma} \tilde{f}^2(A_m^\sigma)}$$

where  $N(A_m^\sigma)$  represents the number of classes of configurationally equivalent clusters in  $A_m$ .

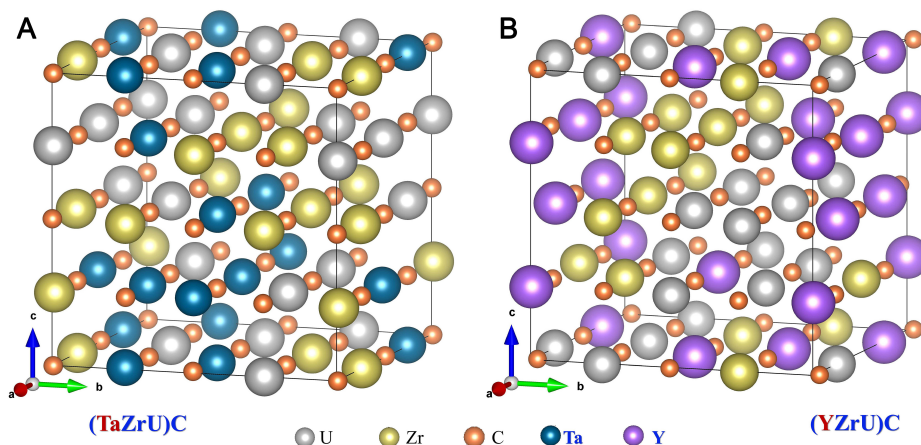


**Figure 1.** The 64 atoms supercells of investigated medium-entropy carbides (MECs) generated by the SAE method. (A) (TaZrU)C; (B) (YZrU)C.

### Computational methods

The first-principles calculations were carried out using the Vienna ab initio simulation package (VASP), which is based on the density functional theory (DFT) framework<sup>[65]</sup>. To treat the interactions between valence electrons and ionic cores, the projector augmented wave (PAW) method was utilized<sup>[66]</sup>, and the exchange-correlation energy was calculated using the generalized gradient approximation (GGA) parametrized by Perdew-Burke-Ernzerh (PBE)<sup>[67]</sup>. Throughout the present work, the plane-wave basis energy cut-off was set to 1.4 times the maximum energy of each component. During the optimization, the total energies calculated by VASP finally converged within  $1 \times 10^{-6}$  eV/atom, and the Monkhorst-Pack scheme<sup>[68]</sup> was used to sample special k-points by automatically generating k-points grid in the Brillouin zone. Full relaxation of the supercell is carried out using the Methfessel-Paxton technique<sup>[69]</sup>. The total energy and electronic density of states (DOS) calculations were performed by using the tetrahedron method with Blöchl correction<sup>[70]</sup>. The bulk modulus, equilibrium volume, and the pressure derivative of the bulk modulus were determined from the total energy calculated, and these results were fitted to the four-parameter Birch-Murnaghan (BM4) equation of state (EOS)<sup>[71]</sup>. The bounding charge density ( $\Delta\rho$ ) was defined as<sup>[72]</sup>:

$$\Delta\rho = \rho_{\text{total}} - \rho_{\text{IAM}}$$

Where  $\rho_{\text{total}}$  is the total electron density, and  $\rho_{\text{IAM}}$  is the density related to the superposition of free and unbonded atoms, also known as the Independent Atomic Model (IAM). The Visualization for Electronic and Structural Analysis (VESTA) code was used to generate the isosurface structures of (TMZrU)C with different values of  $\Delta\rho$ <sup>[73]</sup>.

To investigate the thermodynamic properties, the temperature- and volume-dependent Helmholtz free energy is needed, which is calculated in the following form<sup>[74]</sup>:

$$F(V,T) = E_0(V) + F_{el}(V,T) + F_{vib}(V,T) - TS_{conf}(T)$$

where  $E_0$  represents the static energy at 0 K, corresponding to the energy of the ground state when the ion is fixed in its lattice position. Additionally,  $F_{el}$  accounts for the thermal free energy arising from electronic excitation, while  $F_{ion}$  represents the vibrational contribution to the free energy,  $S_{conf}$  is the configuration entropy of the system. The equilibrium structure of a crystal at any given temperature (T) and volume (V) can be determined by minimizing the Helmholtz free energy  $F(V, T)$ . Once the minimum Helmholtz free energy  $F(V, T)$  is determined for a particular T and V, other thermodynamic functions and properties of the crystal can be deduced as implemented. For instance, entropy (S), isothermal bulk modulus ( $B_T$ ), heat capacity at constant volume ( $C_v$ ), and heat capacity at constant pressure ( $C_p$ ) can be calculated accordingly and expressed as<sup>[75]</sup>:

$$E(V, T) = F(V, T) - T \left[ \frac{\partial F(V, T)}{\partial V} \right]_V$$

$$S(V, T) = - \left[ \frac{\partial F(V, T)}{\partial T} \right]_V$$

$$B_T(V, T) = V \left[ \frac{\partial^2 F(V, T)}{\partial V^2} \right]_T$$

All these thermodynamic properties are estimated using the mean-field potential (MFP) method proposed by Wang *et al.*<sup>[76]</sup> and later improved by Song *et al.*<sup>[75]</sup> to extend its applicability to more general cases and complex structural crystals<sup>[77-79]</sup>. This method is suitable for various complex systems and has significant potential for predicting the thermodynamic properties of multicomponent alloys.

## RESULTS AND DISCUSSION

### Structural stability

The structures are optimized through full relaxation to obtain the energies  $E$  of MECs and their binary carbides as a function of volumes  $V$ . A series of energy-volume data points around the equilibrium volume were calculated by minimizing the total energy to optimize the crystal structure. Then, the energy-volume data points of the calculated MECs and their corresponding individual metal binary carbides were fitted using the fourth-order Birch-Murnaghan EOS<sup>[80]</sup>, as shown in [Figure 2](#).

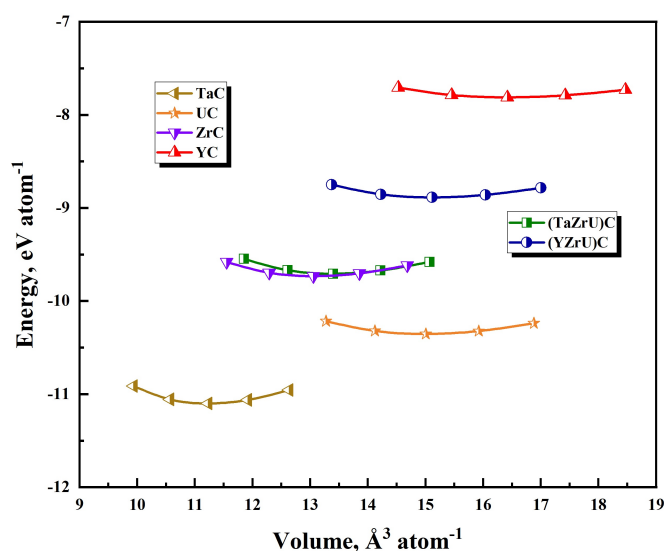
The present results show the effect of TMs on the total energy and volume of MECs. Specifically, the equilibrium volume for binary carbides is found to increase in the order of TaC < ZrC < UC < YC, which is roughly consistent with the trend of pure metal atomic size change, i.e., Ta < U < Zr < Y. In addition, the equilibrium volume of MECs also increases with the increasing volume of TM atoms, in the order of (TaZrU)C < (YZrU)C. Meanwhile, the total energy of middle entropy carbides, (TaZrU)C < (YZrU)C, also increases with the improved volumes of TM atoms.

The fitted E-V curves provide valuable information about the equilibrium atomic energy  $E_0$ , equilibrium volume  $V_0$ , bulk modulus  $B_0$ , first derivative of bulk modulus with respect to pressure  $B_0'$ , and lattice constants  $a$  at zero temperature and pressure for MECs and their corresponding pure carbides. These predicted properties listed in [Table 1](#) are in good agreement with the experimental and theoretical properties reported in the literature<sup>[81-87]</sup>. Specifically, the predicted  $E_0$  and  $V_0$  for (TaZrU)C and (YZrU)C are -9.7095 eV, -8.8862 eV and 13.3873 Å<sup>3</sup>, 15.1241 Å<sup>3</sup>, respectively. The lattice constants are  $a = 9.5097$  Å for (TaZrU)C and  $a = 9.9043$  Å for (YZrU)C. These values are very close to the average values of the equilibrium atomic energies  $E_0$ , equilibrium volumes  $V_0$ , and lattice constants  $a$  of the three component

**Table 1.** The calculated properties of HECs in the present work at ground state (0 K), including equilibrium atomic energy ( $E_0$ ), equilibrium atomic volume ( $V_0$ ), equilibrium bulk modulus ( $B_0$ ), the derivative of  $B_0$  ( $B'$ ), and lattice parameter ( $a$ )

Composition	$E_0$ (eV/atom)	$V_0$ ( $\text{\AA}^3/\text{atom}$ )	$B_0$ (GPa)	$B'$	$a$ ( $\text{\AA}$ )
(TaZrU)C	-9.7059	13.3873	235.14	4.11	9.5097
(YZrU)C	-8.8862	15.1241	173.71	4.45	9.9043
TaC	-11.1001 -11.1 <sup>a</sup> , -11.1 <sup>b</sup>	11.2312	324.88 322.15 <sup>b</sup> , 365.3 <sup>j</sup>	4.23 4.22 <sup>b</sup>	4.48 4.479 <sup>b</sup> , 4.42 <sup>j</sup>
ZrC	-9.7315 -9.74 <sup>a</sup> , -9.73 <sup>b</sup>	13.0724	222.11 219.3 <sup>b</sup> , 220.1 <sup>e</sup>	3.97 4.06 <sup>b</sup>	4.71 4.711 <sup>b</sup> , 4.71 <sup>e</sup>
UC	-10.3533	14.9923	186.77 158 <sup>f</sup> , 191 <sup>g</sup>	3.66	4.93 4.96 <sup>f</sup> , 4.97 <sup>g</sup>
YC	-7.8109	16.4216	123.98 128 <sup>f</sup> , 124.3 <sup>e</sup>	4.06 4.451 <sup>d</sup>	5.08 5.08 <sup>f</sup> , 5.09 <sup>e</sup>

The present first-principles calculations utilize PAW-GGA-PBE. <sup>a</sup>Ye et al., first-principles calculations with PAW-GGA-PBE<sup>[81]</sup>; <sup>b</sup>Jiang et al., first-principles calculations with PAW-GGA-PBE<sup>[82]</sup>; <sup>d</sup>Maibam et al., first-principles calculations with GGA-PBE<sup>[83]</sup>; <sup>e</sup>Korir et al., first-principles calculations with PAW-GGA-PBE<sup>[84]</sup>; <sup>f</sup>Shi et al., first-principles calculations with PAW-GGA-PBE<sup>[85]</sup>; <sup>g</sup>Mei et al., first-principles calculations with PAW-GGA-PBE<sup>[86]</sup>; <sup>j</sup>Isaev et al., first-principles calculations with GGA-PBE<sup>[87]</sup>.

**Figure 2.** The calculated Energy-Volume (E-V) curves of (TaZrU)C and (YZrU)C.

binary carbides. Furthermore, the bulk modulus  $B_0$  of (TaZrU)C and (YZrU)C are also comparable to the average value of the three binary carbides. Similar to most HECs, the equilibrium properties of MECs, (TaZrU)C and (YZrU)C, follow the mixture rule<sup>[88]</sup>, as seen in their equilibrium atomic energy, volume, lattice constant, and bulk modulus.

Mechanical properties are critical to the industrial applications of materials. Interestingly, (TaZrU)C has a greater bulk modulus  $B_0$  than (YZrU)C, indicating that (TaZrU)C has a higher strength than (YZrU)C and will be validated by the following bonding charge density analysis. However, the first derivative of bulk modulus with respect to pressure  $B_0'$  of (TaZrU)C is smaller than that of (YZrU)C. Despite the absence of experimental data for comparison, the current findings can serve as valuable references for future experimental and theoretical research.

### Temperature-dependent thermo-physical properties

The investigation of the thermodynamic properties of materials is crucial in the field of high-temperature engineering applications. In order to gain a deeper understanding of the thermodynamic properties of (TaZrU)C and (YZrU)C in the temperature range of 0-2,000 K, the Debye-Gruneisen model implemented in MFP<sup>[76]</sup> was utilized in this study. The calculated thermodynamic properties are presented in Table 2, including the equilibrium volume  $V_0$ , Gibbs free energy, constant volume heat capacity  $C_v$ , constant pressure heat capacity  $C_p$ , bulk modulus  $B_0$ , and thermal conductivities. The thermodynamic properties of materials can be determined through various experimental techniques, including differential thermal analysis<sup>[60]</sup>, chemical analysis<sup>[89]</sup>, and X-ray diffraction<sup>[61,90,91]</sup>. Additionally, the hardness of a material is commonly measured using Vickers hardness, which can be determined using a nanometer indentation method<sup>[82]</sup>. However, with the advancement of science and technology towards extreme conditions, it becomes increasingly challenging to experimentally obtain accurate thermodynamic data. As a result, there are currently no available experimental or theoretical data on the thermodynamic properties of (TaZrU)C and (YZrU)C. Therefore, the present findings are of significant value in guiding future research efforts to develop advanced NTP fuels.

The heat capacity is a fundamental parameter that links the thermodynamic and dynamic properties of materials. The constant volume heat capacity  $C_v$  was estimated using an expression  $C_v = T \left( \frac{\partial S}{\partial T} \right)_V$  and investigated its temperature dependence for (TaZrU)C and (YZrU)C together with the benchmarks of binary ones, as shown in Figures 3 and 4. In particular, Figure 3 illustrates the constant pressure heat capacity  $C_p$  and constant volume heat capacity  $C_v$  of binary carbides, matching well with the available reported results in the literature and indicating the precise of our benchmark tests. Moreover, the thermodynamic properties of (TaZrU)C and (YZrU)C are presented in Figure 4. In addition, the contributions of ionic and electronic heat capacities are also shown in Figure 4A and B for comparison. The results demonstrate that the ionic heat capacity outweighs the electronic heat capacity across the entire temperature range examined. Compared to the binary carbides of each component, (TaZrU)C and (YZrU)C have larger  $C_p$  and  $C_v$  values due to the mixing of the binary carbides of each component in the same temperature range. It is indicated that these two MECs exhibit a sharp increase in  $C_v$  at temperatures below 400 K, which is also followed by a gradual increase toward a constant value at higher temperatures in line with the Dulong-Petit limit. Notably, the  $C_v$  values of both carbides were very similar at lower temperatures, while the  $C_v$  of (YZrU)C at higher temperatures is slightly higher than that of (TaZrU)C. On the contrary, the  $C_p$  of (TaZrU)C and (YZrU)C is depicted in Figure 4B, and although they exhibit similar trends, their  $C_p$  values are more sensitive to temperature at low temperatures and gradually increase at high temperatures. Furthermore, (YZrU)C displays a larger  $C_p$  than that of (TaZrU)C. It is noteworthy that at very high temperatures,  $C_p$  does not follow the Dulong-Petit law as  $C_v$  does but still shows a small increase. This feature may arise from the relationship between  $C_p$  and  $C_v$  with the expression of  $C_p = C_v + 3\alpha^2 BTv$ .

Estimating the strength of materials is crucial for their practical applications, and the bulk modulus  $B$  is a measure of resistance to compression of a material. An increase in bulk modulus leads to a stronger material. The bulk modulus is calculated using  $B_0 = -V \left( \frac{\partial p}{\partial V} \right)_T$ , and the results for (TaZrU)C and (YZrU)C are displayed in Figure 4C. Both carbides exhibit a significant decrease in bulk modulus with increasing temperature, indicating a more pronounced softening effect. The bulk modulus of (TaZrU)C is consistently higher than that of (YZrU)C throughout the entire temperature range of 0-2,000 K, providing a significant strength advantage of (TaZrU)C in engineering applications.

Entropy is a fundamental thermodynamic parameter that describes the degree of disorder in a crystal structure. A higher entropy value indicates a higher degree of disorder in the crystal structure. The entropy value is a crucial factor for defining HEMs, and its variation is related to the formation, stability, and phase

**Table 2.** Based on quasiharmonic approximation, thermodynamic properties of (TaZrU)C and (YZrU)C predicted by first-principles calculations, including equilibrium volume ( $V_0$ ), Internal energy, Gibbs free energy, Constant volume heat capacity ( $C_v$ ), Constant pressure heat capacity ( $C_p$ ), and Isothermal bulk modulus ( $B_0$ )

Composition	$V_0$ ( $\text{\AA}^3/\text{atom}$ )	Internal (eV)	Gibbs (eV)	$C_v$ (J/mol/K)	$C_p$ (J/mol/K)	$B_0$ (GPa)
(TaZrU)C	13.446	-9.6614	-9.7428	23.098	23.412	228.34
(YZrU)C	15.211	-8.8405	-8.9249	23.174	23.610	167.46

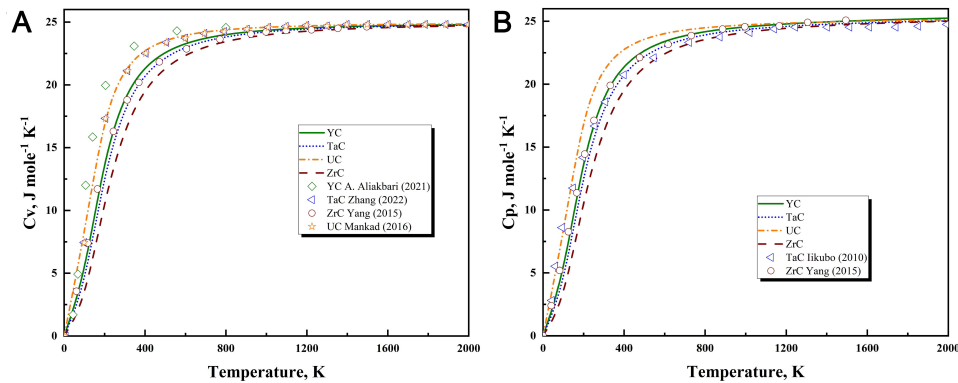


**Figure 3.** Temperature dependence of heat capacity of benchmark binary carbides together with available reported data. (A) Constant volume heat capacity  $C_v$ ; (B) Constant pressure heat capacity  $C_p$ . The values for comparison are derived from the theoretical results reported by Aliakbari<sup>[93]</sup>, Zhang<sup>[94]</sup>, Yang<sup>[57]</sup>, Mankad<sup>[95]</sup>, and Iikubo<sup>[96]</sup>.

transformation of such materials. The equilibrium entropy is calculated using  $S = -(\frac{\partial F}{\partial T})_V$ , and the results are presented in Figure 4D. It can be observed that the entropy curves of those two middle entropy ceramics are close at low temperatures, but (YZrU)C displays a higher entropy than that of (TaZrU)C at high temperatures. Attributing to the differences in the atomic radius and the valence electrons between Ta and Y, these Y atoms in (YZrU)C play a greater influence than Ta when revealing the coupling effects of lattice vibrations and thermal electron contributions to entropy. Based on the relationship between Gibbs free energy Figure 4E and entropy ( $G = U + PV - TS$ ), it can be concluded that (YZrU)C will be more stable at high temperatures.

The theoretical thermal conductivity can be calculated according to the following equation<sup>[92]</sup>:

$$\kappa = A \cdot \frac{M_\alpha \theta_\alpha \delta}{\gamma^2 T}$$

where  $A = 3.04 \times 10^{-8}$ ,  $M_\alpha$  is the atomic mass of the atom,  $\theta_\alpha$  is the Debye temperature,  $\delta^3$  is the volume per atom, and  $\gamma$  is the Gruneisen parameter. Figure 5 shows the corresponding graphs of the thermal conductivities of (TaZrU)C and (YZrU)C. It can be seen from the obtained results that the thermal conductivity trends of (TaZrU)C and (YZrU)C are similar to each other. For the heavier element Ta, the thermal conductivity of the compound (TaZrU)C is larger than that of (YZrU)C. Moreover, the difference in thermal conductivity decreases at high temperatures, and the thermal conductivity of (TaZrU)C is larger than that of (YZrU)C. The reason for this is that the strength of Ta-C bonds is higher than that of Y-C bonds in similar crystal structures, and the covalent interactions in (YZrU)C are weaker than those in (TaZrU)C.

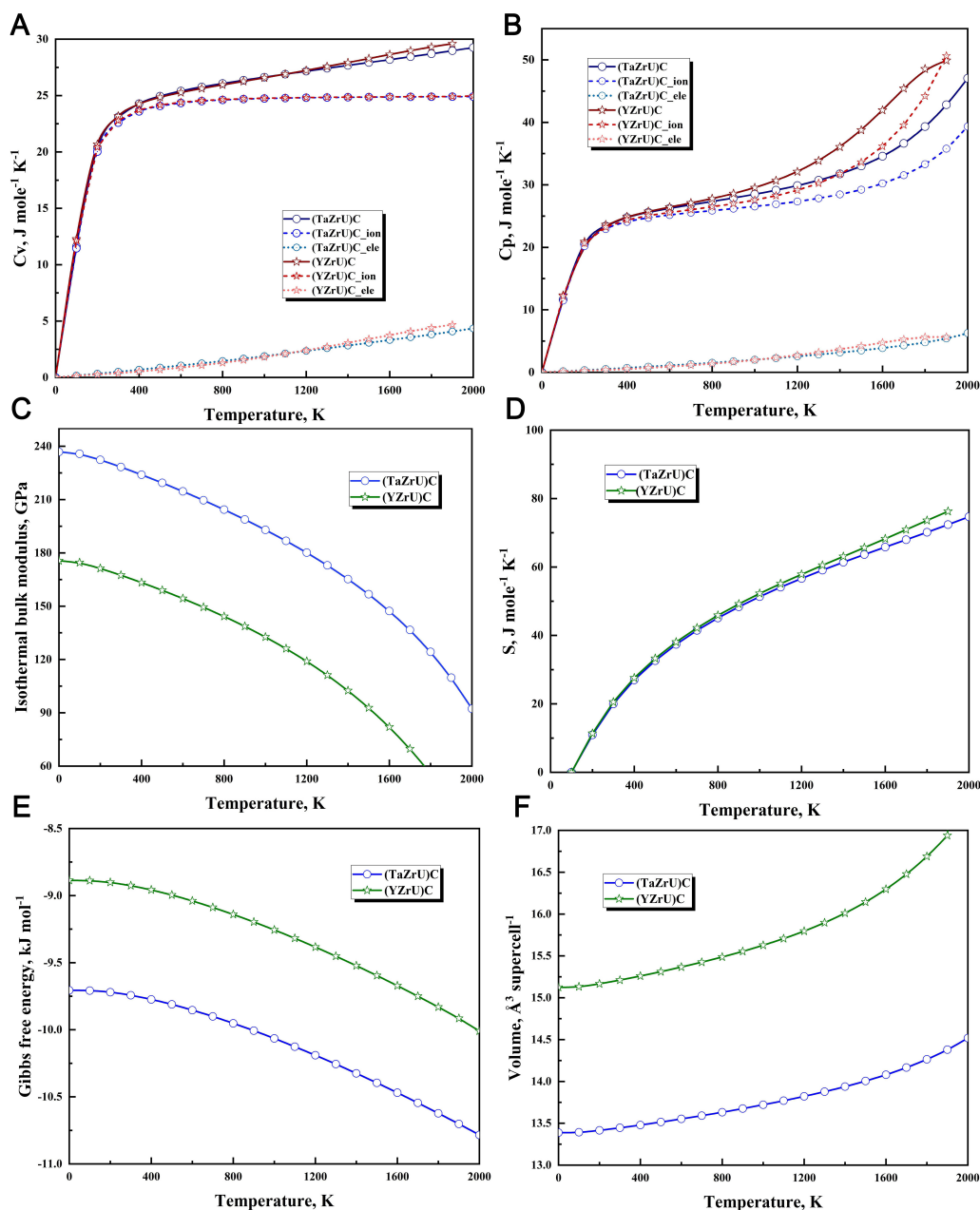


**Figure 4.** The predicted temperature-dependent thermodynamic properties of (TaZrU)C and (YZrU)C. (A) Constant volume heat capacity -  $C_v$ ; (B) Constant pressure heat capacity -  $C_p$ ; (C) Isothermal bulk modulus -  $B$ ; (D) Entropy -  $S$ ; (E) Gibbs free energy; (F) Equilibrium volume.

### Basic physical properties and mechanical properties

Lattice distortion is a crucial microstructural feature that affects the mechanical properties of materials, especially in high-entropy materials. From the perspective of bond charge density, the mechanical and chemical effects of lattice distortion/misfit caused by constituent atoms can be comprehensively characterized. Figure 6 shows the isosurface of bonding charge densities of MECs with  $\Delta\rho = 0.016 e^{-\text{Å}^{-3}}$ , demonstrating the electronic rearrangement caused by solute atoms and lattice distortion. The red color indicates the loss of electrons, while the green color represents the gain of electrons. Additionally, Figure 7A-D presents the electron gain and loss situations for (TaZrU)C and (YZrU)C, respectively. The results demonstrate that chemical disorder and lattice distortion in MECs can disturb the electronic

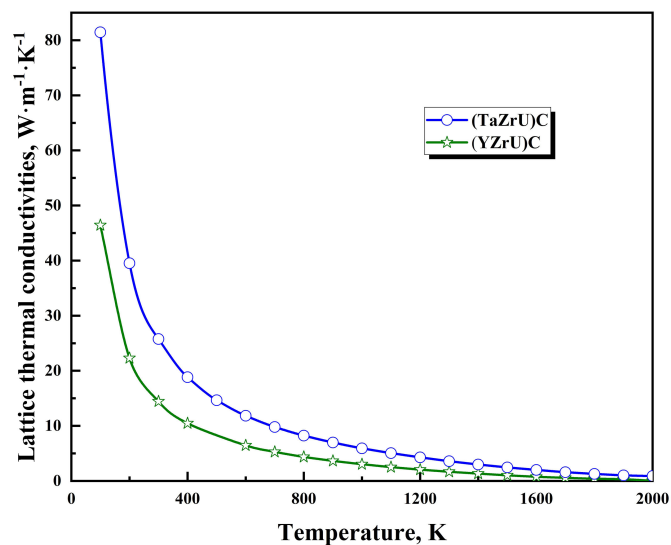


**Figure 5.** The temperature-dependent lattice thermal conductivity of (TaZrU)C and (YZrU)C.

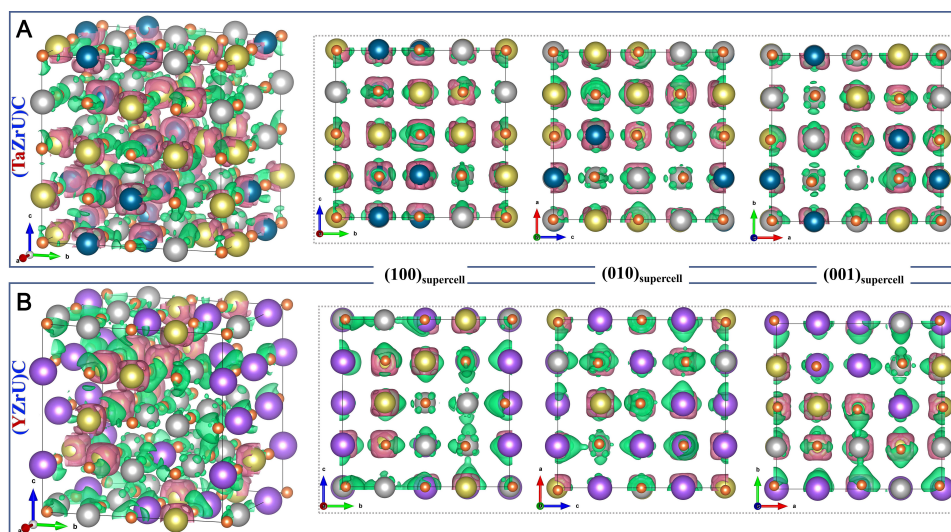


**Figure 6.** The chemical bonding of investigated medium entropy carbides (MECs) characterized by the 3D and 2D views of bonding charge density isosurfaces ( $\Delta\rho = 0.016 \text{ e}^{-} \text{ \AA}^{-3}$ ), (A) (TaZrU)C; (B) (YZrU)C. The green and the pink colors are utilized to highlight those atoms presenting the negative and the positive charge, respectively.

contributions. In those investigated medium entropy ceramics, metal atoms exhibit different degrees of electron gain and loss, with the order of the metal atoms receiving electrons being  $U > Y$  while the order of metal atoms losing electrons being  $Ta > Zr$ . This observation suggests that metal atoms in MECs experience varying degrees of electron gain and loss, which increase as their atomic size decreases. Since the higher  $\Delta\rho$  density corresponds to the stronger chemical bonds, it can be inferred that the hardness of (TaZrU)C is larger than that of (YZrU)C, which is consistent with the analysis of the partial bulk modulus  $B_0$  in the previous section on thermodynamic properties.

In order to gain a deeper understanding of the bonding behavior of the two MECs, we conducted an analysis of the charge density distribution on the (001) plane, and contour plots are shown in Figure 8. It

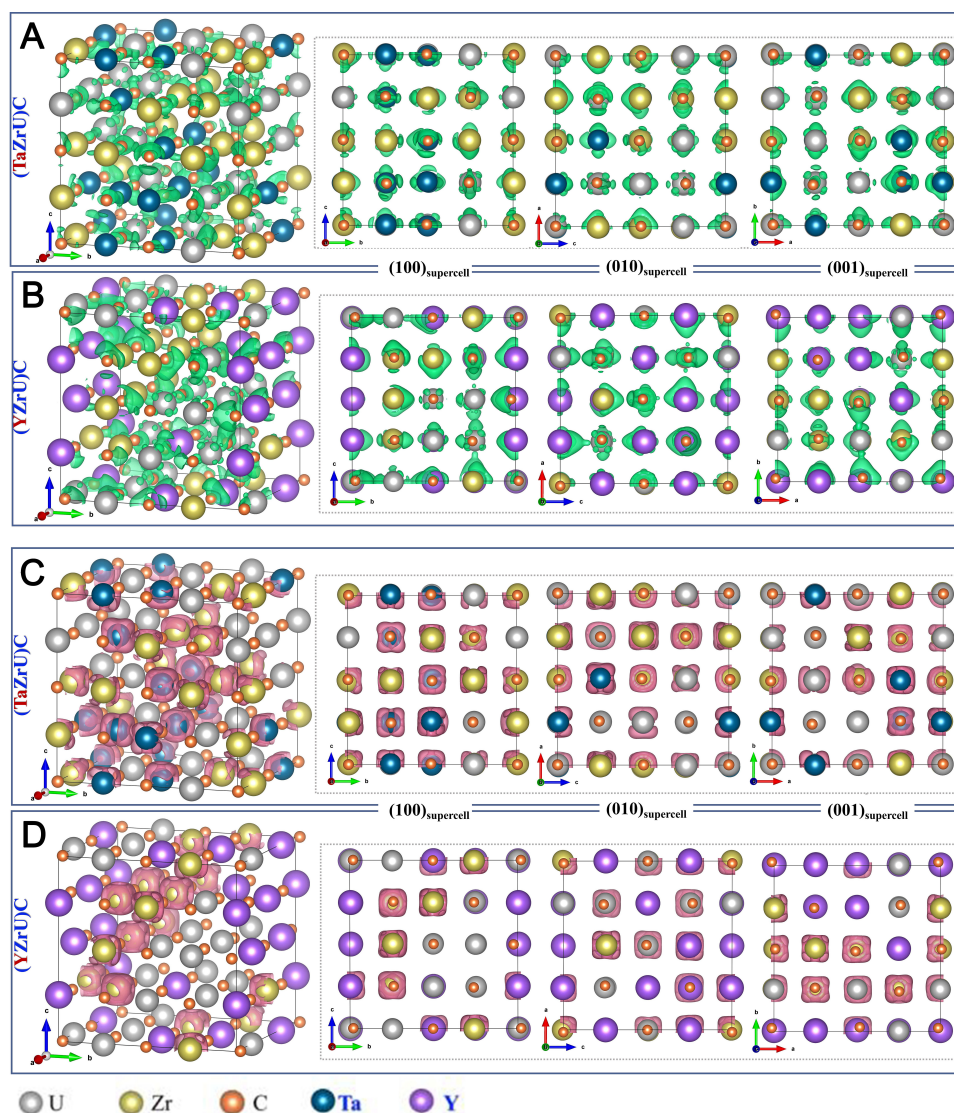


**Figure 7.** The chemical bonding of investigated medium entropy carbides (MECs) in the views of individual positive and negative modules of bonding charge density isosurfaces, (A) and (C) the negative and positive charge of (TaZrU)C, respectively; (B) and (D) the negative and positive charge of (YZrU)C, respectively.

can be seen from the figure that the charge distribution is strongly perturbed by the chemical disorder. In particular, we observed significant hybridization between the carbon and TM atoms, which suggests the formation of covalent bonds between them. Interestingly, the charge overlap region between TM atoms and non-metal atoms in (TaZrU)C is noticeably wider and more delocalized than that in (YZrU)C. Additionally, the color between TM and carbon atoms in (TaZrU)C is orange, whereas it is yellow and green in (YZrU)C. This observation suggests that the enhanced bonding charge densities among those atoms in (TaZrU)C result in increased bonding strength between TM and carbon atoms. As a consequence, the hardness of (TaZrU)C will be further enhanced, which is consistent with the findings from the analysis of  $\Delta\rho$  from both 3D and 2D perspectives.

The DOS is a crucial quantity in theoretical chemistry as it helps to understand the internal chemical bond interactions and the stability mechanisms of a compound structure. To gain a deeper understanding of the

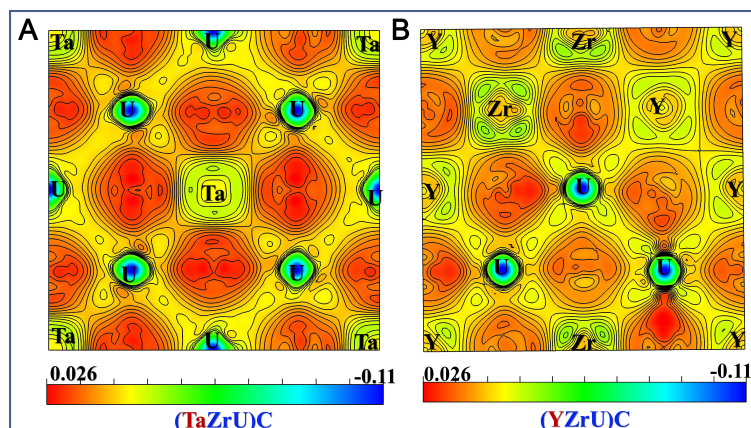


**Figure 8.** The contour plots of bonding charge density distributions of (001) plane of medium entropy carbides (MECs), (A) (TaZrU)C and (B) (YZrU)C. In order to get a clearer view of the electron distribution in the diagram, only the position of metal atoms has been marked, while the position of C atoms has not been marked, which is between two metal atoms. Plots are generated by the Visualization for Electronic and Structural Analysis (VESTA) package.

electronic structure, bonding, and properties of (TaZrU)C and (YZrU)C, their total (TDOS) and partial DOS (PDOS) are shown in Figure 9. The vertical blue line in the figure marks the Fermi energy ( $E_F$ ) which has been set to zero. Figure 9A shows that both MECs have TDOS values above zero at the Fermi energy level  $N(E_F)$ , indicating clear metallic behavior. However, (YZrU)C exhibits a smaller deviation between its Fermi level and pseudo-gap, and the DOS at the Fermi level is also smaller than (TaZrU)C. This indicates that (YZrU)C is more stable, as a lower DOS at the Fermi level  $N(E_F)$  means higher stability. Due to the similarities in the PDOS details between (TaZrU)C and (YZrU)C, (TaZrU)C is chosen as the prototype for further analysis. As shown in Figure 9B, the two main peaks are located between -3 and 1 eV, with the Fermi energy approximately in the middle of this range. The primary bonding peaks located between -5 and -3 eV are predominantly derived from the valence electrons of the C(p), U(f), Ta(d), and Zr(d) orbitals. Meanwhile, the bonding peaks between -3 eV and 1 eV are generated through the hybridization of the C(p), U(f), Ta(d), and Zr(d) orbitals, with a minor contribution from the U(d), Ta(p), and Zr(p) orbitals. These PDOS features indicate the presence of covalent-like bonds in (TaZrU)C. Similarly, (YZrU)C exhibits the same PDOS features.

## CONCLUSION

In the present work, the electronic and thermodynamic properties of (TaZrU)C and (YZrU)C have been investigated by first-principles calculations, referring to the traditional binary carbides, such as TaC, ZrC, UC, and YC, and presenting a good agreement with available experimental or theoretical results in the literature. It is found that the equilibrium volume and energy of (TaZrU)C and (YZrU)C are positively correlated with the size of each solute atom. Due to the random occupation of TM elements, local lattice distortion occurs, leading to changes in the charge distribution and chemical bonds. The electron DOS ( $\epsilon$ DOS) displays the bonding ability of the two MECs, showing significant hybridization between the carbon and the TM atoms near the Fermi level, indicating the formation of covalent bonds. The predicted bonding structures in view of bonding charge density indicate that (TaZrU)C and (YZrU)C exhibit covalent characteristics accompanied by ionicity, with (TaZrU)C showing stronger covalent interactions. Based on the Debye-Grüneisen model, several fundamental properties of (TaZrU)C and (YZrU)C were further studied, including constant volume and constant pressure heat capacities, bulk modulus, thermodynamic entropy, Gibbs free energy, volume, and thermal conductivity. While the high-temperature softening behavior is similar in those investigated carbides, (TaZrU)C has stronger chemical bonds and greater

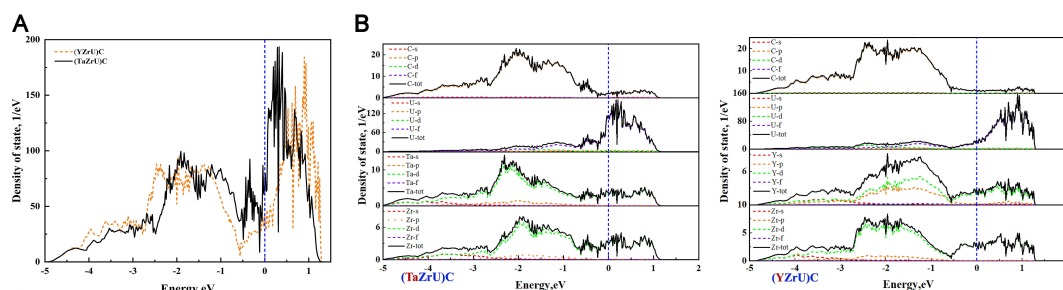


**Figure 9.** (A) Total electron density of states (TDOS) and (B) Partial electron density of states (PDOS) of (TaZrU)C and (YZrU)C. The blue vertical dotted lines at 0 eV dictate the Fermi level.

hardness due to its larger volume modulus and thermal conductivity, making it more suitable for engineering applications. Since the entropy was found to increase significantly with temperature for both carbides, (YZrU)C becomes more stable at high temperatures due to its greater contribution from entropy. Therefore, the present work provides some reference value for the optimization and application of future medium entropy ceramic NTP fuels.

## DECLARATIONS

### Authors' contributions

Investigation, Methodology, Calculation, Data curation, Analysis, Writing - original draft, Writing - review and editing: Liu Y

Conceptualization, Methodology, Investigation, Resources, Writing - original draft, Writing - review and editing, Supervision, Funding acquisition: Wang WY

Investigation, Data curation, Analysis, Writing - review and editing: Li J

Conceptualization, Methodology, Software: Zhang Y

Conceptualization, Methodology, Software, Data curation, Analysis: Yin J

Conceptualization, Methodology, Supervision, Writing - review and editing: Pan X, Gao X, Chen Y, Song H, Lu Y

Resources, Writing - review and editing, Project administration, Funding acquisition: Li J

### Availability of data and materials

Not applicable.

### Financial support and sponsorship

This work was financially supported by the National Defense Basic Scientific Research (2022-JCKY-JJ-1086). First-principles calculations were carried out on the clusters at Northwestern Polytechnical University.

### Conflicts of interest

All authors declared that there are no conflicts of interest.

### Ethical approval and consent to participate

Not applicable.

### Consent for publication

Not applicable.

## Copyright

© The Author(s) 2023.

## REFERENCES

1. Nisar A, Zhang C, Boesl B, Agarwal A. A perspective on challenges and opportunities in developing high entropy-ultra high temperature ceramics. *Ceram Int* 2020;46:25845-53. DOI
2. Akrami S, Edalati P, Fuji M, Edalati K. High-entropy ceramics: review of principles, production and applications. *Mater Sci Eng R Rep* 2021;146:100644. DOI
3. Demirskiy D, Borodianska H, Suzuki TS, Sakka Y, Yoshimi K, Vasylykiv O. High-temperature flexural strength performance of ternary high-entropy carbide consolidated via spark plasma sintering of TaC, ZrC and NbC. *Scr Mater* 2019;164:12-6. DOI
4. Golla BR, Mukhopadhyay A, Basu B, Thimmappa SK. Review on ultra-high temperature boride ceramics. *Prog Mater Sci* 2020;111:100651. DOI
5. Peters AB, Zhang D, Nagle DC, Spicer JB. Reactive two-step additive manufacturing of ultra-high temperature carbide ceramics. *Addit Manuf* 2023;61:103318. DOI
6. Ni D, Cheng Y, Zhang J, et al. Advances in ultra-high temperature ceramics, composites, and coatings. *J Adv Ceram* 2022;11:1-56. DOI
7. Dai F, Wen B, Sun Y, Ren Y, Xiang H, Zhou Y. Grain boundary segregation induced strong UHTCs at elevated temperatures: a universal mechanism from conventional UHTCs to high entropy UHTCs. *J Mater Sci Technol* 2022;123:26-33. DOI
8. Guo R, Mao H, Shen P. Ultra-fast high-temperature synthesis and densification of high-entropy diborides and diboride-carbide ceramics. *J Eur Ceram Soc* 2023;43:5763-73. DOI
9. Morris BA, Povolny SJ, Seidel GD, Tallon C. Effects of oxidation on the effective thermomechanical properties of porous ultra-high temperature ceramics in compression via computational micromechanics and MPM. *Open Ceram* 2023;15:100382. DOI
10. Oses C, Toher C, Curtarolo S. High-entropy ceramics. *Nat Rev Mater* 2020;5:295-309. DOI
11. Wei X, Liu J, Li F, Qin Y, Liang Y, Zhang G. High entropy carbide ceramics from different starting materials. *J Eur Ceram Soc* 2019;39:2989-94. DOI
12. Zhou J, Zhang J, Zhang F, Niu B, Lei L, Wang W. High-entropy carbide: a novel class of multicomponent ceramics. *Ceram Int* 2018;44:22014-8. DOI
13. Yan X, Constantin L, Lu Y, Silvain J, Nastasi M, Cui B.  $(\text{Hf}_{0.2}\text{Zr}_{0.2}\text{Ta}_{0.2}\text{Nb}_{0.2}\text{Ti}_{0.2})\text{C}$  high-entropy ceramics with low thermal conductivity. *J Am Ceram Soc* 2018;101:4486-91. DOI
14. Zeng Y, Wang D, Xiong X, et al. Ablation-resistant carbide  $\text{Zr}_{0.8}\text{Ti}_{0.2}\text{C}_{0.74}\text{B}_{0.26}$  for oxidizing environments up to 3,000 °C. *Nat Commun* 2017;8:15836. DOI PubMed PMC
15. Csanádi T, Castle E, Reece MJ, Dusza J. Strength enhancement and slip behaviour of high-entropy carbide grains during micro-compression. *Sci Rep* 2019;9:10200. DOI PubMed PMC
16. Wang F, Yan X, Wang T, et al. Irradiation damage in  $(\text{Zr}_{0.25}\text{Ta}_{0.25}\text{Nb}_{0.25}\text{Ti}_{0.25})\text{C}$  high-entropy carbide ceramics. *Acta Mater* 2020;195:739-49. DOI
17. Yeh J, Chen S, Lin S, et al. Nanostructured high-entropy alloys with multiple principal elements: novel alloy design concepts and outcomes†. *Adv Eng Mater* 2004;6:299-303. DOI
18. Ma J, Huang C. High entropy energy storage materials: synthesis and application. *J Energy Storage* 2023;66:107419. DOI
19. Ying T, Yu T, Qi Y, Chen X, Hosono H. High entropy van der Waals materials. *Adv Sci* 2022;9:e2203219. DOI PubMed PMC
20. Moghaddam A, Fereidonnejad R, Cabot A. Semi-ordered high entropy materials: the case of high entropy intermetallic compounds. *J Alloys Compd* 2023;960:170802. DOI
21. Yao G, Wang W, Li P, et al. Electronic structures and strengthening mechanisms of superhard high-entropy diborides. *Rare Met* 2023;42:614-28. DOI
22. Sarker P, Harrington T, Toher C, et al. High-entropy high-hardness metal carbides discovered by entropy descriptors. *Nat Commun* 2018;9:4980. DOI PubMed PMC
23. Yao G, Wang WY, Zou C, et al. Local orders, lattice distortions, and electronic structure dominated mechanical properties of  $(\text{ZrHfTaM1M2})\text{C}$  (M = Nb, Ti, V). *J Am Ceram Soc* 2022;105:4260-76. DOI
24. Dai F, Wen B, Sun Y, Xiang H, Zhou Y. Theoretical prediction on thermal and mechanical properties of high entropy  $(\text{Zr}_{0.2}\text{Hf}_{0.2}\text{Ti}_{0.2}\text{Nb}_{0.2}\text{Ta}_{0.2})\text{C}$  by deep learning potential. *J Mater Sci Technol* 2020;43:168-74. DOI
25. Kaufmann K, Maryanovsky D, Mellor WM, et al. Discovery of high-entropy ceramics via machine learning. *npj Comput Mater* 2020;6:42. DOI
26. Chen L, Chen Z, Yao X, et al. High-entropy alloy catalysts: high-throughput and machine learning-driven design. *J Mater Inf* 2022;2:19. DOI
27. Zhou Y, Zhang Z, Wang D, et al. New trends in additive manufacturing of high-entropy alloys and alloy design by machine learning: from single-phase to multiphase systems. *J Mater Inf* 2022;2:18. DOI
28. Chen Z, Yang Y. Data-driven design of eutectic high entropy alloys. *J Mater Inf* 2023;3:10. DOI
29. Pak AY, Sotskov V, Gumovskaya AA, et al. Machine learning-driven synthesis of  $\text{TiZrNbHfTaC}_3$  high-entropy carbide. *npj Comput Mater* 2023;9:7. DOI

30. Castle E, Csanádi T, Grasso S, Dusza J, Reece M. Processing and properties of high-entropy ultra-high temperature carbides. *Sci Rep* 2018;8:8609. DOI PubMed PMC
31. Dusza J, Švec P, Girman V, et al. Microstructure of (Hf-Ta-Zr-Nb)C high-entropy carbide at micro and nano/atomic level. *J Eur Ceram Soc* 2018;38:4303-7. DOI
32. Xiong K, You L, Zhang S, et al. Pressure and temperature effects on (TiZrTa)C medium-entropy carbide from first-principles. *J Mater Res Technol* 2023;23:2288-300. DOI
33. Jin C, Xiong K, Guo L, et al. A DFT insight into the mechanical, electronic and thermodynamic properties of (TiZrHf)C medium-entropy carbide ceramic. *Results Phys* 2022;35:105341. DOI
34. Demirskiy D, Suzuki TS, Yoshimi K, Vasylykiv O. Synthesis and high-temperature properties of medium-entropy (Ti,Ta,Zr,Nb)C using the spark plasma consolidation of carbide powders. *Open Ceram* 2020;2:100015. DOI
35. Demirskiy D, Nishimura T, Suzuki TS, Sakka Y, Vasylykiv O, Yoshimi K. High-temperature toughening in ternary medium-entropy (Ta<sub>1/3</sub>Ti<sub>1/3</sub>Zr<sub>1/3</sub>)C carbide consolidated using spark-plasma sintering. *J Asian Ceram Soc* 2020;8:1262-70. DOI
36. Peng C, Tang H, He Y, et al. A novel non-stoichiometric medium-entropy carbide stabilized by anion vacancies. *J Mater Sci Technol* 2020;51:161-6. DOI
37. Deng H, Xie Z, Wang M, et al. A nanocrystalline AlCoCuNi medium-entropy alloy with high thermal stability via entropy and boundary engineering. *Mater Sci Eng A* 2020;774:138925. DOI
38. Chen H, Xiang H, Dai F, et al. High porosity and low thermal conductivity high entropy (Zr<sub>0.2</sub>Hf<sub>0.2</sub>Ti<sub>0.2</sub>Nb<sub>0.2</sub>Ta<sub>0.2</sub>)C. *J Mater Sci Technol* 2019;35:1700-5. DOI
39. Peng C, Gao X, Wang M, et al. Diffusion-controlled alloying of single-phase multi-principal transition metal carbides with high toughness and low thermal diffusivity. *Appl Phys Lett* 2019;114:011905. DOI
40. Wang Y, Csanádi T, Zhang H, Dusza J, Reece MJ, Zhang R. Enhanced Hardness in high-entropy carbides through atomic randomness. *Adv Theory Simul* 2020;3:2000111. DOI
41. Ye B, Wen T, Chu Y. High-temperature oxidation behavior of (Hf<sub>0.2</sub>Zr<sub>0.2</sub>Ta<sub>0.2</sub>Nb<sub>0.2</sub>Ti<sub>0.2</sub>)C high-entropy ceramics in air. *J Am Ceram Soc* 2020;103:500-7. DOI
42. Wang Y, Zhang R, Zhang B, et al. The role of multi-elements and interlayer on the oxidation behaviour of (Hf-Ta-Zr-Nb)C high entropy ceramics. *Corros Sci* 2020;176:109019. DOI
43. Levack DJ, Horton JF, Jennings T, et al. Evolution of low enriched uranium nuclear thermal propulsion vehicle and engine design. In: AIAA Propulsion and Energy 2019 Forum; 2019 Aug 19-22; Indianapolis, IN, USA. American Institute of Aeronautics and Astronautics, Inc.; 2019. p. 3943. DOI
44. Reynolds CB, Horton JF, Joyner CR, Kokan T, Levack DJ. Applications of nuclear thermal propulsion to lunar architectures. In: AIAA Propulsion and Energy 2019 Forum; 2019 Aug 19-22; Indianapolis, IN, USA. American Institute of Aeronautics and Astronautics, Inc.; 2019. p. 4032. DOI
45. Ji Y, Zhang H, Sun J, Shi L. Thermal performance optimization of a fuel element in particle bed reactors for nuclear thermal propulsion. *Nucl Eng Des* 2019;355:110316. DOI
46. Reynolds CB, Joyner CR, Kokan TS, Levack DJ, Muzek BJ. Mars opposition missions using nuclear thermal propulsion. In: AIAA Propulsion and Energy 2020 Forum; 2020 Aug 24-28; virtual event. American Institute of Aeronautics and Astronautics, Inc.; 2020. p. 3850. DOI
47. Burns D, Johnson S. Nuclear thermal propulsion reactor materials. In: Nuclear Materials. IntechOpen; 2021. Available from: <https://www.intechopen.com/chapters/71396>. [Last accessed on 16 Aug 2023].
48. Lin CS, Youinou GJ. Design and analysis of a 250 MW plate-fuel reactor for nuclear thermal propulsion. Available from: <https://www.osti.gov/biblio/1638498>. [Last accessed on 15 Aug 2023].
49. Thody A. Irradiation capsule development for composite fuels for nuclear thermal propulsion. Available from: [https://ir.library.oregonstate.edu/concern/graduate\\_thesis\\_or\\_dissertations/6395wd417](https://ir.library.oregonstate.edu/concern/graduate_thesis_or_dissertations/6395wd417). [Last accessed on 15 Aug 2023]
50. Searight WT, Palomares KB, Werner JE, Todosow M, Lenox KE. Subscale maturation of advanced reactor technologies (SMART): a path forward for nuclear thermal propulsion fuel and reactor development. *Prog Nucl Energy* 2022;153:104432. DOI
51. Wang SB, Ma Y, Guo SM, Xie QL. Comparison and analysis of nuclear thermal propulsion reactor fuel. *Manned Spaceflight* 2018; 24:784-95. (in Chinese). Available from: <http://www.cnki.net/kcms/doi/10.16329/j.cnki.zrht.2018.06.012.html>. [Last accessed on 15 Aug 2023].
52. Farhadizadeh AR, Ghomi H. Mechanical, structural, and thermodynamic properties of TaC-ZrC ultra-high temperature ceramics using first principle methods. *Mater Res Express* 2020;7:036502. DOI
53. Tsuppayakorn-aek P, Ektarawong A, Sukmas W, Alling B, Bovornratanaraks T. Thermodynamic stability and superconductivity of tantalum carbides from first-principles cluster expansion and isotropic Eliashberg theory. *Comput Mater Sci* 2022;202:111004. DOI
54. Di Y, He Z, Wang J. New insights into the mechanical and thermal properties of UN<sub>1-x</sub>C<sub>x</sub> from first-principles calculations. *J Nucl Mater* 2022;571:153991. DOI
55. Gökbulut M, Koç H, Bölükdemir MH, Eser E. Analytical study of the heat capacity and entropy of ZrM (M=N and C) compounds. *Int J Mod Phys B* 2023;2450276. DOI
56. He R, Fang L, Han T, et al. Elasticity, mechanical and thermal properties of polycrystalline hafnium carbide and tantalum carbide at high pressure. *J Eur Ceram Soc* 2022;42:5220-8. DOI
57. Yang XY, Lu Y, Zheng FW, Zhang P. Mechanical, electronic, and thermodynamic properties of zirconium carbide from first-principles calculations. *Chin Phys B* 2015;24:116301. DOI

58. Pelaccio DG, El-Genk MS, Butt DP. A review of carbide fuel corrosion for nuclear thermal propulsion applications. *Am Inst Phys* 1994;301:905-18. [DOI](#)
59. Wu XZ, Wei GL, Guo X. Study on preparation technology and performance mechanism of multi-component (U,Zr,Nb)C fuel. *Sci Technol At Energy* 2023;9:1-9. (in Chinese) Available from: <http://kns.cnki.net/kcms/detail/11.2044.tl.20230626.1905.008.html>. [Last accessed on 15 Aug 2023]
60. Butt DP, Wallace TC. The U-Zr-C ternary phase diagram above 2473 K. *J Am Ceram Soc* 1993;76:1409-19. [DOI](#)
61. Bourgeois L, Dehaut P, Lemaignan C, Hammou A. Factors governing microstructure development of Cr<sub>2</sub>O<sub>3</sub>-doped UO<sub>2</sub> during sintering. *J Nucl Mater* 2001;297:313-26. [DOI](#)
62. Koroteev AS. Nuclear propulsion system application in the space exploration. In: The 10th International Burn and Combustion Summit (2003).
63. Tian F, Lin DY, Gao X, Zhao YF, Song HF. Erratum: "a structural modeling approach to solid solutions based on the similar atomic environment" [J. Chem. Phys. 153, 034101 (2020)]. *J Chem Phys* 2020;153:034101. [DOI](#) [PubMed](#)
64. Song H, Tian F, Hu Q, et al. Local lattice distortion in high-entropy alloys. *Phys Rev Mater* 2017;1:023404. [DOI](#)
65. Kresse G, Furthmüller J. Efficient iterative schemes for *ab initio* total-energy calculations using a plane-wave basis set. *Phys Rev B* 1996;54:11169-86. [DOI](#) [PubMed](#)
66. Blöchl PE. Projector augmented-wave method. *Phys Rev B* 1994;50:17953-79. [DOI](#) [PubMed](#)
67. Perdew JP, Burke K, Ernzerhof M. Generalized gradient approximation made simple. *Phys Rev Lett* 1996;77:3865-8. [DOI](#) [PubMed](#)
68. Monkhorst HJ, Pack JD. Special points for Brillouin-zone integrations. *Phys Rev B* 1976;13:5188-92. [DOI](#)
69. Methfessel M, Paxton AT. High-precision sampling for Brillouin-zone integration in metals. *Phys Rev B* 1989;40:3616-21. [DOI](#) [PubMed](#)
70. Blöchl PE, Jepsen O, Andersen OK. Improved tetrahedron method for Brillouin-zone integrations. *Phys Rev B* 1994;49:16223-33. [DOI](#) [PubMed](#)
71. Murnaghan FD. The Compressibility of media under extreme pressures. *Proc Natl Acad Sci U S A* 1944;30:244-7. [DOI](#) [PubMed](#) [PMC](#)
72. Nakashima PN, Smith AE, Etheridge J, Muddle BC. The bonding electron density in aluminum. *Science* 2011;331:1583-6. [DOI](#) [PubMed](#)
73. Momma K, Izumi F. *VESTA 3* for three-dimensional visualization of crystal, volumetric and morphology data. *J Appl Cryst* 2011;44:1272-6. [DOI](#)
74. Ma D, Grabowski B, Körmann F, Neugebauer J, Raabe D. *Ab initio* thermodynamics of the CoCrFeMnNi high entropy alloy: importance of entropy contributions beyond the configurational one. *Acta Mater* 2015;100:90-7. [DOI](#)
75. Song H, Liu H. Modified mean-field potential approach to thermodynamic properties of a low-symmetry crystal: beryllium as a prototype. *Phys Rev B* 2007;75:245126. [DOI](#)
76. Wang Y, Li L. Mean-field potential approach to thermodynamic properties of metal: Al as a prototype. *Phys Rev B* 2000;62:196-202. [DOI](#)
77. Wang Y, Xu Y, Liu Y, et al. First-principles study of the role of surface in the heavy-fermion compound CeRh<sub>2</sub>Si<sub>2</sub>. *Phys Rev B* 2021;103:165140. [DOI](#)
78. Wu J, Yang Z, Xian J, Gao X, Lin D, Song H. Structural and thermodynamic properties of the high-entropy alloy AlCoCrFeNi based on first-principles calculations. *Front Mater* 2020;7:590143. [DOI](#)
79. Wu J, Wang YC, Liu Y, et al. First-principles study on the electronic structure transition of β-UH<sub>3</sub> under high pressure. *Matter Radiat Extrem* 2022;7:058402. [DOI](#)
80. Birch F. Finite strain isotherm and velocities for single-crystal and polycrystalline NaCl at high pressures and 300°K. *J Geophys Res* 1978;83:1257-68. [DOI](#)
81. Ye B, Wen T, Nguyen MC, Hao L, Wang C, Chu Y. First-principles study, fabrication and characterization of (Zr<sub>0.25</sub>Nb<sub>0.25</sub>Ti<sub>0.25</sub>V<sub>0.25</sub>)C high-entropy ceramics. *Acta Mater* 2019;170:15-23. [DOI](#)
82. Jiang S, Shao L, Fan T, Duan J, Chen X, Tang B. Elastic and thermodynamic properties of high entropy carbide (HfTaZrTi)C and (HfTaZrNb)C from *ab initio* investigation. *Ceram Int* 2020;46:15104-12. [DOI](#)
83. Maibam J, Indrajit Sharma B, Bhattacharjee R, Thapa R, Brojen Singh R. Electronic structure and elastic properties of scandium carbide and yttrium carbide: a first principles study. *Phys B Condens Matter* 2011;406:4041-5. [DOI](#)
84. Korir K, Amolo G, Makau N, Joubert D. First-principle calculations of the bulk properties of 4d transition metal carbides and nitrides in the rocksalt, zincblende and wurtzite structures. *Diam Relat Mater* 2011;20:157-64. [DOI](#)
85. Shi H, Zhang P, Li S, Sun B, Wang B. Electronic structures and mechanical properties of uranium monocarbide from first-principles LDA + U and GGA + U calculations. *Phys Lett A* 2009;373:3577-81. [DOI](#)
86. Mei Z, Ye B, Yacout AM, Beeler B, Gao Y. First-principles study of the surface properties of uranium carbides. *J Nucl Mater* 2020;542:152257. [DOI](#)
87. Isaev EI, Simak SI, Abrikosov IA, et al. Phonon related properties of transition metals, their carbides, and nitrides: a first-principles study. *J Appl Phys* 2007;101:123519. [DOI](#)
88. Zhao Y, Qiao J, Ma S, et al. A hexagonal close-packed high-entropy alloy: the effect of entropy. *Mater Des* 2016;96:10-5. [DOI](#)
89. Wang Z, Qiu W, Yang Y, Liu C. Atomic-size and lattice-distortion effects in newly developed high-entropy alloys with multiple principal elements. *Intermetallics* 2015;64:63-9. [DOI](#)
90. Viennois R, Bérardan D, Popescu C. Crystal structure, lattice dynamics, and thermodynamic properties of a thermoelectric

- orthorhombic BaCu<sub>2</sub>Se<sub>2</sub> compound. *J Phys Chem C* 2020;124:13627-38. DOI
91. Wen T, Ye B, Nguyen MC, Ma M, Chu Y. Thermophysical and mechanical properties of novel high-entropy metal nitride-carbides. *J Am Ceram Soc* 2020;103:6475-89. DOI
  92. Watari K, Shinde SL. High thermal conductivity materials. *MRS Bull* 2001;26:440-4. DOI
  93. Aliakbari A, Amiri P. Structural, elastic, electronic, thermal, and phononic properties of yttrium carbide: first-principles calculations. *Mater Chem Phys* 2021;270:124744. DOI
  94. Zhang P, Ye L, Chen F, Han W, Wu Y, Zhao T. Stability, mechanical, and thermodynamic behaviors of (TiZrHfTaM)C (M = Nb, Mo, W, V, Cr) high-entropy carbide ceramics. *J Alloy Compd* 2022;903:163868. DOI
  95. Mankad VH, Jha PK. Thermodynamic properties of nuclear material uranium carbide using density functional theory. *J Therm Anal Calorim* 2016;124:11-20. DOI
  96. Iikubo S, Ohtani H, Hasebe M. First-principles calculations of the specific heats of cubic carbides and nitrides. *Mater Trans* 2010;51:574-7. DOI